RECORD
2022/17

CRYSTALLINE BASEMENT BENEATH THE EASTERN CANNING BASIN AT THE TOP UP RISE PROSPECT

DE Kelsey, MTD Wingate, CV Spaggiari, RH Smithies,
IOH Fielding, Y Lu, JK Porter and EG Finch

Government of **Western Australia**
Department of **Mines, Industry Regulation and Safety**

Geological Survey of Western Australia

Government of **Western Australia**
Department of **Mines, Industry Regulation and Safety**

RECORD 2022/17

CRYSTALLINE BASEMENT BENEATH THE EASTERN CANNING BASIN AT THE TOP UP RISE PROSPECT

DE Kelsey, MTD Wingate, CV Spaggiari[1], RH Smithies, IOH Fielding, Y Lu, JK Porter[2,3] and EG Finch[4]

1 Centre of Excellence in Natural Resource Management, The University of Western Australia, Albany WA 6330
2 MinEx CRC, Australian Resources Research Centre (ARRC), 26 Dick Perry Avenue, Kensington WA 6151
3 Future Industries Institute, University of South Australia, Mawson Lakes SA 5090
4 ANSTO, 800 Blackburn Road, Clayton VIC 3168

PERTH 2022

Geological Survey of Western Australia

MINISTER FOR MINES AND PETROLEUM
Hon Bill Johnston MLA

DIRECTOR GENERAL, DEPARTMENT OF MINES, INDUSTRY REGULATION AND SAFETY
Richard Sellers

EXECUTIVE DIRECTOR, GEOLOGICAL SURVEY AND RESOURCE STRATEGY
Michele Spencer

REFERENCE
The recommended reference for this publication is:
Kelsey, DE, Wingate, MTD, Spaggiari, CV, Smithies, RH, Fielding, IOH, Lu, Y, Porter, JK and Finch, EG 2022, Crystalline basement beneath the eastern Canning Basin at the Top Up Rise prospect: Geological Survey of Western Australia, Record 2022/17, 16p.

ISBN 978-1-74168-993-8
ISSN 2204-4345

Grid references in this publication refer to the Geocentric Datum of Australia 1994 (GDA94). Locations mentioned in the text are referenced using Map Grid Australia (MGA) coordinates, Zone 52. All locations are quoted to at least the nearest 100 m.

EXPLORATION INCENTIVE SCHEME
John de Laeter Centre
MinEx CRC

Isotope and element analyses were conducted using the SHRIMP ion microprobe facilities at the John de Laeter Centre (JdLC), Curtin University, with the financial support of the Australian Research Council and AuScope National Collaborative Research Infrastructure Strategy (NCRIS).

Published 2022 by the Geological Survey of Western Australia
This Record is published in digital format (PDF) and is available online at <www.dmirs.wa.gov.au/GSWApublications>.

Further details of geoscience products are available from:
First Floor Counter
Department of Mines, Industry Regulation and Safety
100 Plain Street
EAST PERTH WESTERN AUSTRALIA 6004
Telephone: +61 8 9222 3459 Email: publications@dmirs.wa.gov.au
www.dmirs.wa.gov.au/GSWApublications

Cover image: Journey to the centre of the Kimberley (© 2010 PL Schubert)

Contents

Figures

Tables

Crystalline basement beneath the eastern Canning Basin at the Top Up Rise prospect

DE Kelsey, MTD Wingate, CV Spaggiari[1], RH Smithies, IOH Fielding, Y Lu, JK Porter[2,3], and EG Finch[4]

Abstract

Exploration drillcores from the Top Up Rise prospect are currently the only available basement rocks to study within the Lasseter Shear Zone system that underlies the eastern Canning Basin, west of the Aileron Province of the North Australian Craton (NAC). Varied lithologies include upper amphibolite to lower granulite facies metasedimentary and granitic schists and gneisses (including in situ and injected leucosomes), amphibolites, metagabbros and metadolerites. Alteration and sulfide mineralization attest to at least two hydrothermal fluid flow events. SHRIMP (Sensitive High-Resolution Ion Microprobe) U–Pb zircon geochronology indicates mainly 1880–1870 Ma zircon cores in metagranitic rocks, interpreted as xenocrystic, and 3074–1825 Ma cores in metasedimentary rocks, with maximum depositional ages of the protoliths of 1877–1852 Ma. Zircon rims in all samples yield dates of 1624–1604 Ma, interpreted as the time of granitic magmatism during upper amphibolite to lower granulite facies metamorphism. This interpretation is based on: (a) truncation of concentric zoning in zircon cores in metagranitic samples; (b) the peraluminous to strongly peraluminous geochemistry of metagranitic samples, in which inherited zircon is to be expected; (c) centimetre-scale to metre-scale interlayering of leucosome with host rock and the absence of larger granitic intrusions; (d) no obvious basement–cover relationships in the drillcore to suggest 1880–1870 Ma basement onto which sediments were deposited; and (e) preservation of rare intrusive contacts between leucosome and metasedimentary rock. Zircons with ages ranging from 1880 to 1870 Ma are common detrital components in 1865–1835 Ma metasedimentary rocks across the NAC, and Top Up Rise prospect zircon age spectra are very similar to the 'Detrital P' signature (i.e. dominated by Paleoproterozoic ages) of the NAC. This indicates that the NAC continues westwards beneath the easternmost Canning Basin, at least as far as the Lasseter Shear Zone. Although the rocks at Top Up Rise prospect may not be a source for 1880–1870 Ma zircons across the NAC, significant and widespread 1880–1870 Ma granitic sources presumably exist and are yet to be discovered. Massive metagabbro and olivine metagabbro were emplaced at c. 968 Ma, and metadolerites are younger than c. 968 Ma. The geological evolution of the Top Up Rise prospect was protracted, and the latest events included high-strain deformation that overprinted earlier (1852–1624 Ma) hydrothermal and alteration activity, including sulfide mineralization. It is possible that mylonitization could be Neoproterozoic or Paleozoic in age.

KEYWORDS: basement, drillcore, geochronology, geological history, granitic rock, metasediments, Precambrian, Proterozoic

Introduction

This Record documents the rock types and contact relationships in diamond drillcores from crystalline basement beneath the far eastern Canning Basin, from the Top Up Rise prospect (Fig. 1). These drillcores are interpreted to intersect the Lasseter Shear Zone system, which truncates the dominant east-trending structures of the North Australian Craton (NAC) — specifically those in the Aileron and Warumpi Provinces — and likely represents their western extent. The Top Up Rise prospect is above a distinct northeast-trending gravity ridge bound by northeast-trending shear zones coincident with the Lasseter Shear Zone (Fig. 1; Braun et al., 1991). The drillcores contain partially melted or melt-injected upper-amphibolite to low-granulite facies basement rocks. These are currently the only drillcores that intersect basement to the Canning Basin in this region and they provide a means to test its tectonic affinity, and the significance of the Lasseter Shear Zone.

The Top Up Rise prospect is in the Gibson Desert of eastern Western Australia, on the WILSON 1:250 000 map sheet (SF52-09) and TOP UP RISE 1:100 000 map sheet (4352), and within the Kiwirrkurra Indigenous Protected Area. The nearest major centre is Alice Springs, about 700 km to the east, and Kiwirrkurra Community is 40 km to the east-southeast. Access to the prospect is via gravel road about 42 km to the west of Kiwirrkurra, then on community and historical exploration tracks. The tenement of the Top Up Rise prospect was named Desert Road EL 80/4427 and operated by a joint venture between Border Exploration Pty Ltd and Corazon Mining Limited (Marshall, 2013). There is no rock outcrop and the physiography is typical of an arid environment, dominated by vegetated sandy plains and dunes (Marshall, 2013). In this tenement, Border Exploration Pty Ltd conducted a combined air core, reverse circulation and diamond drilling program in 2012 and 2013, with 2475.1 m drilled. The drilling was co-funded under the Western Australian government's Exploration Incentive Scheme (EIS). A summary of the diamond drilling from Marshall (2013) is provided in Table 1, and the drillhole locations are shown in Figure 1.

1 Centre of Excellence in Natural Resource Management, The University of Western Australia, Albany WA 6330

2 MinEx CRC, Australian Resources Research Centre (ARRC), 26 Dick Perry Avenue, Kensington WA 6151

3 Future Industries Institute, University of South Australia, Mawson Lakes SA 5090

4 ANSTO, 800 Blackburn Road, Clayton VIC 3168

Geological background

Basement intersected beneath overlying Canning Basin sediments in Top Up Rise prospect drillcores is similar in age to the Aileron and Warumpi Provinces, as outlined below. The Aileron and Warumpi Provinces outcrop mostly in the Northern Territory but continue westwards for about 175 km into Western Australia (Hollis et al., 2013). The older Aileron Province is to the north of the Warumpi Province (Fig. 1).

The Aileron Province is characterized by metasedimentary and magmatic rocks, with the majority of the protolith ages between c. 1860 and 1700 Ma (e.g. Scrimgeour, 2013a). Magmatic events — involving both felsic and mafic magmatism — are numerous and include the 1810–1800 Ma Stafford, 1780–1760 Ma Yambah, 1755–1740 Ma Inkamulla, 1735–1690 Ma Strangways and 1690–1650 Ma Argilke Events, the 1640–1630 Ma Liebig Orogeny and 1590–1550 Ma Chewings Event (e.g. Scrimgeour, 2013a; Beyer, 2017). Major periods of sedimentation occurred at 1865–1830 Ma (Lander Rock Formation and equivalents) and 1810–1780 Ma (Reynolds Range Group and correlatives) (Scrimgeour, 2013a; Maidment et al., 2020). Metasedimentary rocks of the Lander Rock Formation and equivalents are widely considered to be the oldest known rocks of the Aileron Province (Scrimgeour, 2013a). However, rare magmatic rocks older than the c. 1860 Ma Lander Rock Formation outcrop at the margins of the Entia Dome (Beyer et al., 2013), an inlier of Aileron Province in the east of the Northern Territory, and may represent basement to the Aileron Province supracrustal rocks. Maidment et al. (2020, 2022) recognized that 1865–1835 Ma metasedimentary rocks of

Table 1. Summary of diamond drillholes by Border Exploration Pty Ltd within their tenement EL 80/4427 as part of their Top Up Rise project. More details can be found in the final drilling report by Marshall (2013)

Hole ID	*Northing (m)*	*Easting (m)*	*Dip (°)*	*Azimuth (°)*	*Total depth (m)*	*Pre-collar hole ID*	*Pre-collar total depth (m)*
TUR13DD001	7499769	337513	-70	090	279.7	TUR13RC002	149.0
TUR13DD002	7497800	339400	-60	090	328.4	TUR13RC004	208.0
TUR13DD003	7497798	339159	-60	090	816.3	TUR13RC003	283.0
TUR13DD004	7503072	338397	-90	090	669.8	TUR13RC005	202.0
TUR13DD005	7499158	340071	-60	090	369.6	TUR13RC006	201.0

NOTE: UTM coordinates are Zone 52

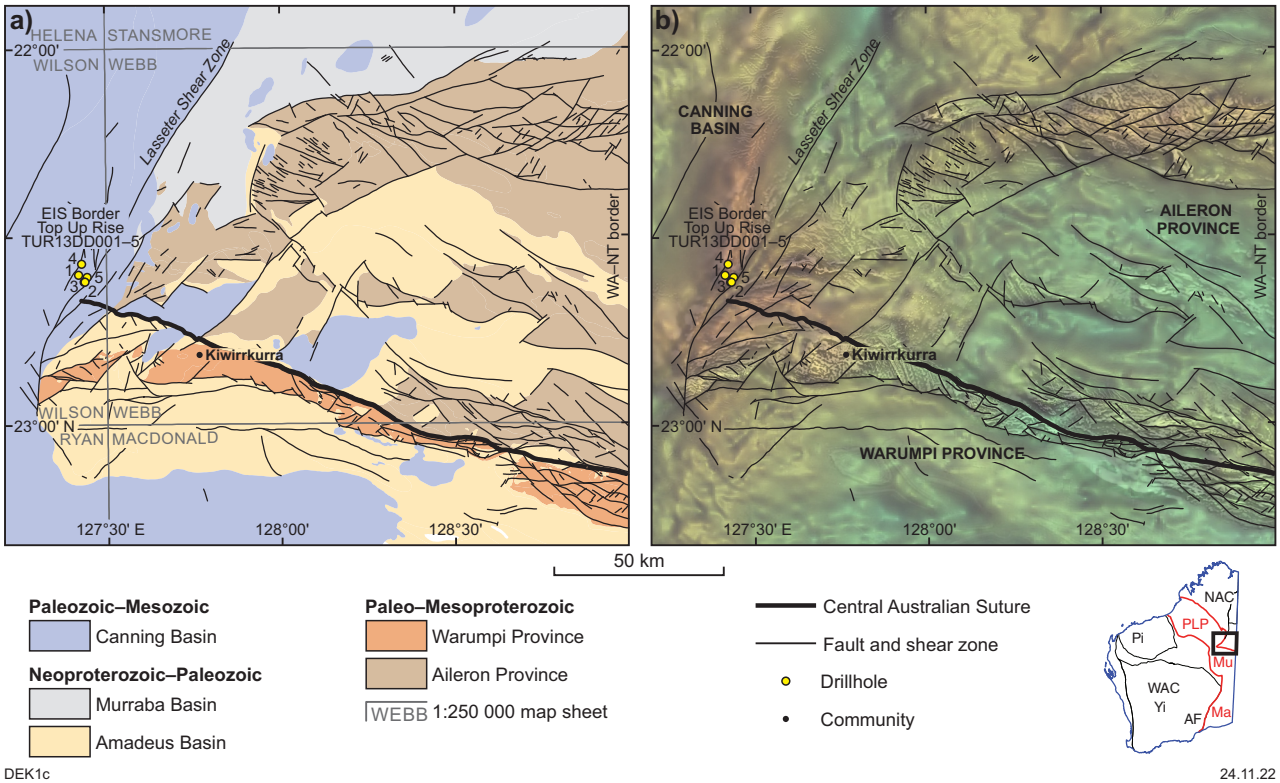

Figure 1. Simplified map of tectonic units (a) showing the Top Up Rise prospect drillcores within the Lasseter Shear Zone system, which defines the major eastern boundary of the Canning Basin and the western boundary of the Aileron and Warumpi Provinces. The gravity image (b) shows the northeast-trending ridge bound by northeast-trending shear zones coincident with the Lasseter Shear Zone. Modified from Hollis et al. (2013). Inset showing State tectonic domains adapted from Lu et al. (2022). Abbreviations for inset: AF, Albany–Fraser Orogen; Ma, Madura Province; Mu, Musgrave Province; NAC, North Australian Craton; Pi, Pilbara Craton; PLP, Percival Lakes Province; WAC, West Australian Craton; Yi, Yilgarn Craton. Black box in inset shows location of the main images

both the Aileron Province and NAC have a distinct detrital zircon age signature, comprising minor Archean to earliest Paleoproterozoic ages, and a dominant 1880– 1865 Ma age component. This defines the so-called 'Detrital P' metasedimentary packages (Maidment et al., 2020).

In the Warumpi Province, magmatic and volcanic events occurred at 1690–1660, 1640–1630 and 1600–1610 Ma, sedimentation at 1660–1650 and 1630–1610 Ma, and metamorphism and migmatization at 1640–1630 and 1150–1100 Ma (e.g. Scrimgeour, 2013b; Wong et al., 2015). The abundant 1690–1610 Ma magmatic and metasedimentary rocks of the Warumpi Province are younger than the majority of rocks in the Aileron Province (Scrimgeour, 2013b). Nevertheless, c. 1640 Ma magmatic rocks and 1880–1770 Ma detrital zircons in the Warumpi Province have isotope compositions that overlap those of Aileron Province crust (Hollis et al., 2013).

The boundary between the Aileron and Warumpi Provinces is the approximately east-trending Central Australian Suture (Fig. 1; Close et al., 2004; Scrimgeour et al., 2005a,b), which has been interpreted to represent the southern margin of the NAC. As such, the Warumpi Province has been interpreted to be exotic to the Aileron Province and the NAC, and to define a paleo-subduction margin (Scrimgeour et al., 2005b). By contrast, Hollis et al. (2013) interpreted the Warumpi Province as a slice of Aileron Province crust that was rifted away at or before c. 1690 Ma and then re-accreted later. In this latter interpretation, the Warumpi Province is not exotic to the NAC and the Central Australian Suture is not a paleo-subduction margin.

To the west, the Central Australian Suture and Warumpi and Aileron Provinces are truncated by the north-northeasterly trending Lasseter Shear Zone system (Fig. 1; Braun et al., 1991). The age of initiation of the Lasseter Shear Zone system is uncertain but is presumably concurrent with or after the 1640–1630 Ma Liebig or 1590–1550 Ma Chewings Orogenies. Younger reactivation events are also likely, including during Ordovician extension and initiation of the Canning Basin (e.g. Martin et al., 2022). The SEEBASE study interpreted the Lasseter Shear Zone system to contain 1085–1030 Ma volcanic rocks of the Giles Suite (Frogtech Geoscience, 2017) although this has not been confirmed.

To the west of the Aileron and Warumpi Provinces, and terminated by the Lasseter Shear Zone, is the main depocentre of the Canning Basin. The Canning Basin is an Ordovician to Cretaceous intracratonic sedimentary basin that occupies about 640,000 km^2 of northwestern Australia (e.g. Zhan, 2018). Immediately west of the Lasseter Shear Zone within the Kidson Sub-basin and Ryan Shelf, the Canning Basin is at least several kilometres deep (Frogtech Geoscience, 2017; Doublier et al., 2020). The Canning Basin onlaps the Aileron and Warumpi Provinces to a thickness of <1 km (Frogtech Geoscience, 2017). Basement underlying the main depocentre of the Canning Basin is buried and largely unknown. However, isotope data from rare intersections of granitic basement underneath the northwestern Canning Basin reveal isotopic affinity with crust analogous to the protolith of the Musgrave Province, Madura Province and eastern Albany–Fraser Orogen, specifically Lu–Hf zircon model ages of 1900–1400 Ma (Lu et al., 2022). This basement beneath the Canning Basin is termed the Percival Lakes Province. Lu et al. (2022) proposed that crust with isotopic character of the Percival Lakes–Musgrave–Madura Provinces and eastern Albany–Fraser Orogen entirely underlies the Canning Basin and is terminated at the Lasseter Shear Zone against the Aileron Province.

Basement lithologies

There are a range of rock types within the five drillcores, encompassing gneisses and migmatites with unknown protoliths, metasedimentary rocks, amphibolites, metagabbro and olivine metagabbro, metagranitic rocks — including metaleucogranites and pegmatites — and late metadolerites that crosscut other rock types (Figs 2–4). In some drillcores, there are intervals up to several metres thick of metamorphosed hydrothermal rocks (Figs 2, 3a) and include thinner intervals of massive sulfide mineralization. Contacts between various rock types are spaced at centimetre-scales to metre-scales (Figs 2, 4). Late, typically discrete hydrothermal alteration consisting of zones or veins containing epidote, quartz, calcite, K-feldspar, chlorite, sulfide minerals and hematite overprint the host rocks (Fig. 4f–h). All five drillholes intersected zones with minor pyrrhotite–chalcopyrite–pyrite±galena±sphalerite± pentlandite mineralization (Fig. 3a), indicating that the area is prospective for metallic ores (Marshall, 2013).

Gneissic fabric is well developed in metasedimentary rocks and in gneisses and migmatites of unknown protolith, as well as in amphibolites and metamorphosed hydrothermal rocks, and some of the metagranitic rocks (Figs 3b–d, 4). More intense and localized deformation, characterized by protomylonite to mylonite, from centimetre-scale to hectometre-scale in width, affects these same rock types (Figs 2, 3e) and the metagabbro and olivine metagabbro (Fig. 3f) and, in some instances, the late metadolerites, indicating that at least some high-strain deformation post-dated all rocks.

Metasedimentary rocks and those with unknown protoliths are typically dominated by biotite, muscovite, quartz and feldspar, and some contain sillimanite and fibrolitic sillimanite, or both (Fig. 3b,c). Garnet is rare in all drillcores, although it is in some pegmatites and granitic gneisses, and also in some amphibolites as spongiform grains (see description of amphibolites below). The abundance of mica in the rocks and absence of peritectic minerals such as garnet, orthopyroxene or cordierite in leucosomes suggests the maximum metamorphic grade is lower granulite facies (Kelsey et al., 2022).

Some gneisses and migmatites for which the protoliths are unknown are likely metasedimentary rocks, whereas others are sufficiently ambiguous, both visually and mineralogically, and may be either meta-igneous ('S-type' granitic) or metasedimentary rocks, or a mix between the two. Whole-rock geochemistry shows that rocks with unknown protolith are mildly to strongly peraluminous (aluminium saturation index, ASI; molar $Al_2O_3/(CaO+Na_2O+K_2O)$ >1.10). These samples have an ASI up to 3.12 (Fig. 5a), consistent with a sedimentary origin or derivation via partial melting of a sedimentary source, although distinction between the two is difficult. Therefore, we apply a conservative classification scheme (i.e. migmatitic gneiss and prefixed micaceous gneisses or schists labels in Fig. 2) rather than attempting to be definitive about the source for these rocks, although we acknowledge that an appreciable (or even total) component of these rocks is probably sedimentary in origin.

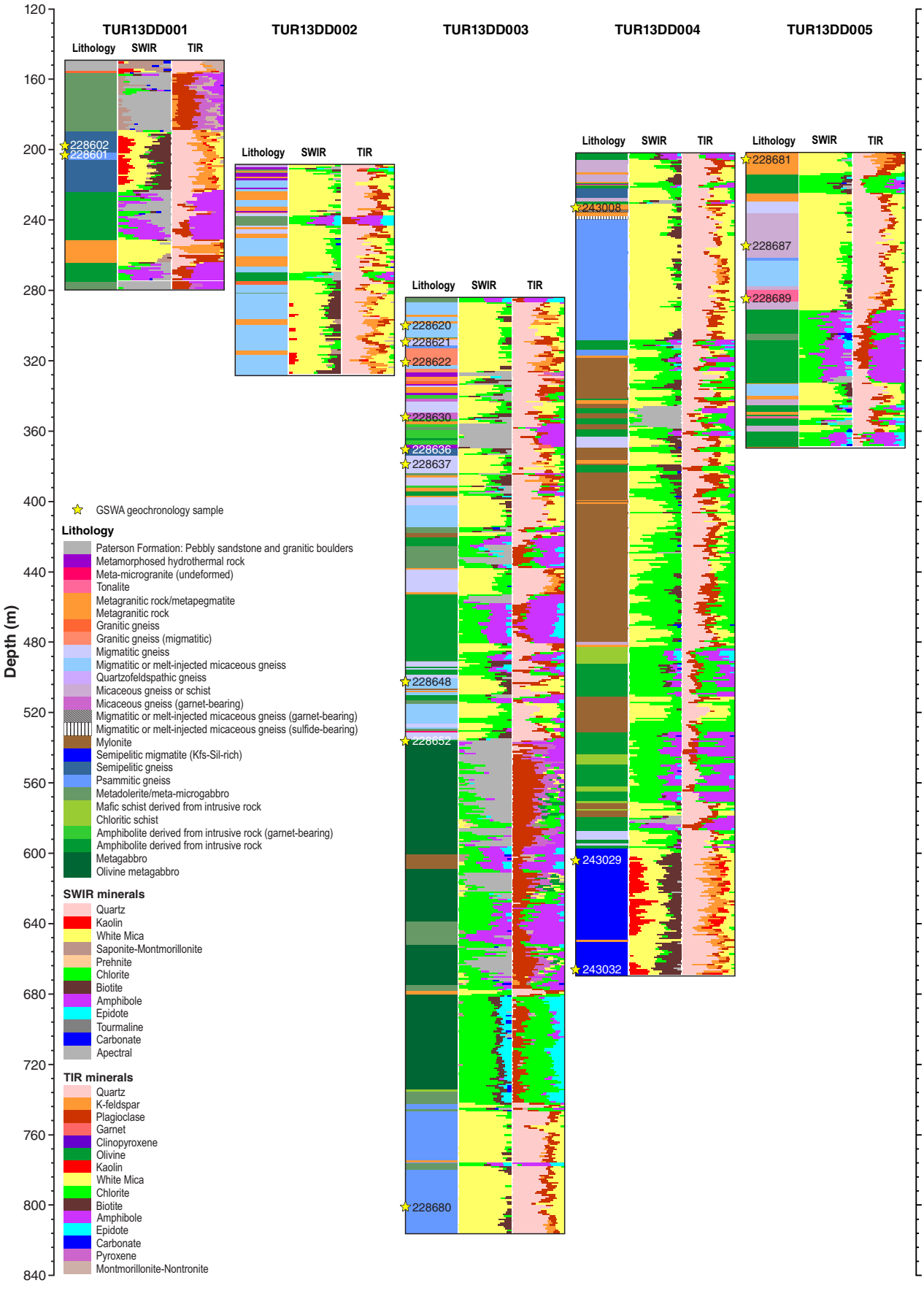

Figure 2. Logs for the five diamond drillcores from the Top Up Rise prospect. The intervals above the logs shown are occupied by the RC pre-collars summarized in Table 1. For each drillcore, the three logs shown are, from left to right, the lithology logged by the authors and the mineralogical summaries of hyperspectral data collected by the GSWA HyLogger spectral scanner, with short-wave infrared (SWIR) summary data in the centre and thermal infrared (TIR) summary data on the right. More HyLogger information and data are available for the drillcores, including photos of rock trays, at geoview.dmp.wa.gov.au/geoview/?Viewer=GeoView and <www.dmirs.wa.gov.au/hylogger>. Locations of GSWA geochronology samples are shown with a yellow star and corresponding sample ID label

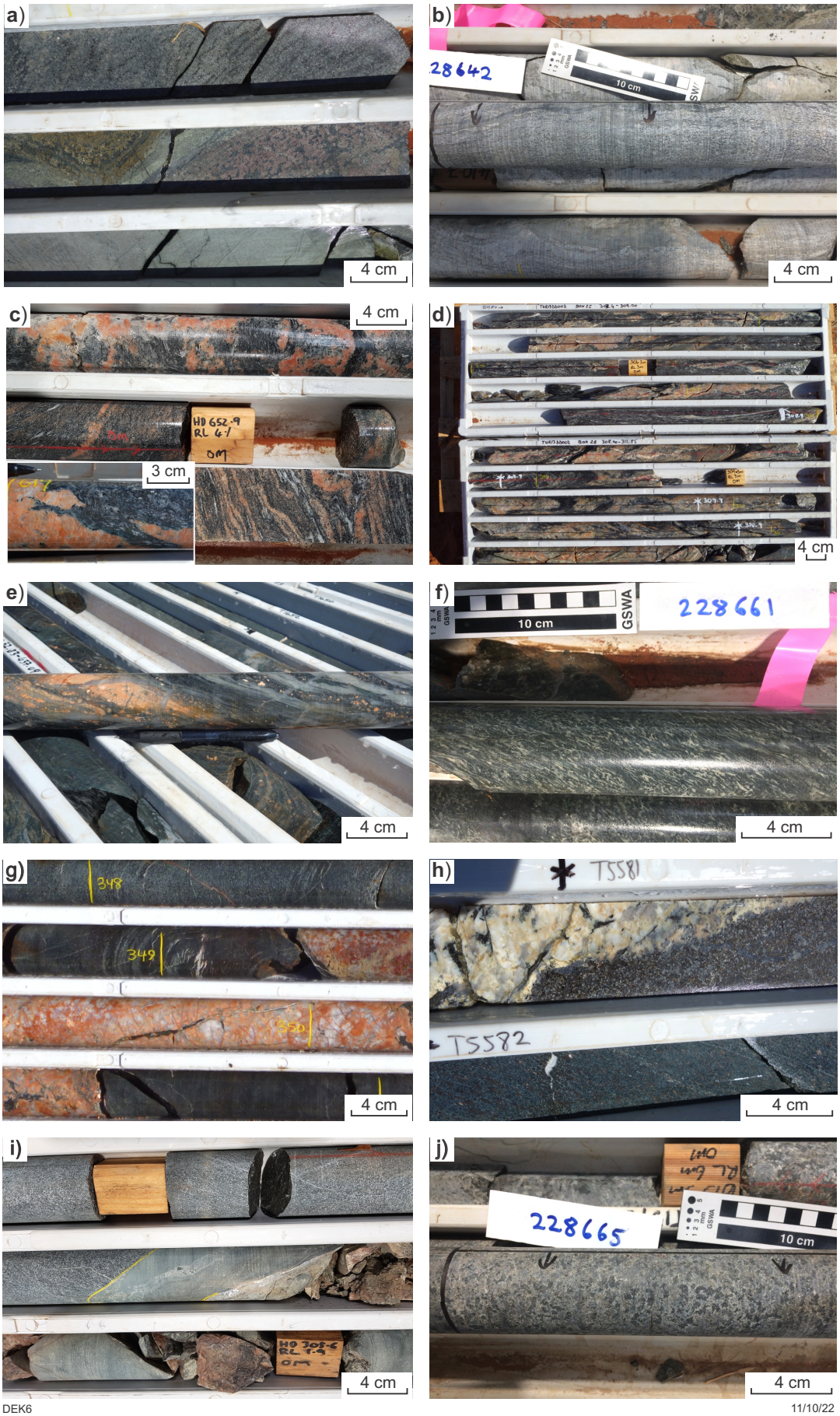
a)
4 cm
b)
28642
10 cm
4 cm
c)
4 cm
HD 652-9
RL 4-7
3 cm
d)
4 cm
e)
4 cm
f)
10 cm
GSWA
228661
4 cm
g)
348
349
350
4 cm
h)
TS581
TS582
4 cm
i)
4 cm
j)
228665
10 cm
4 cm

DEK6 11/10/22

Figure 3 . (page 5) Lithologies and contact relationships in the Top Up Rise prospect drillcores. In all photos, the diameter of drillcore is 47.6 mm. a) Tray 1 (~210.45 – 210.75 m) of TUR13DD002, photo courtesy of David Maidment. Example of sulfide-bearing metamorphosed hydrothermal rock. The rock is compositionally layered, featuring micaceous gneiss (top), layered massive sulfide (pyrrhotite, pyrite and minor chalcopyrite; centre left), garnet–quartz-rich layers (centre right) and diopside–apatite-rich layers (bottom); b) Tray 32 (411.95 m) of TUR13DD003, site of sample GSWA 228642. Peraluminous micaceous gneiss to migmatitic or melt-injected gneiss with anastomosing but well-developed foliation defined by biotite and coarse-grained and fine-grained muscovite, and (local) fibrolitic sillimanite; c) Trays 106–107 (~650.5 to 654.5 m) of TUR13DD004. Semipelitic migmatite—also featuring injected granite—containing abundant muscovite, biotite, sillimanite and orange K-feldspar. Inset from tray 98 (613.6 to 617.9 m) of TUR13DD004, showing sharp-tipped apophyses of granite injected into the semipelitic host; d) Trays 25–26 (303.4 – 311.85 m) of TUR13DD002, photo courtesy of Border Exploration Pty Ltd. Leucocratic layers within typical migmatitic or melt-injected micaceous gneiss. Granitic veins are parallel to discordant to the anastomosing foliation and commonly boudinaged; e) Tray 54, ~431.3 m of TUR13DD004, photo courtesy of David Maidment. Mylonite, in this example affecting metagranite and micaceous (migmatitic or melt-injected) gneiss; f) Tray 76 (597.28 – 597.39 m) of TUR13DD003, site of sample GSWA 228661. Anastomosing protomylonitic to mylonitic deformation fabric within coarse-grained metagabbro–meta-olivine gabbro; g) Tray 34 (~347.90 – 351.05 m) of TUR13DD005. Coarse-grained pegmatite–granite with strong orange colour intruding foliated amphibolite. This granite features coarse, abundant books of euhedral muscovite (bottom left of photo and see also Fig. 4a for same drillcore tray). The amphibolite has discrete zones of alteration to epidote and actinolite; h) Tray 27 (~264.10 m) of TUR13DD001, photo courtesy of David Maidment. Biotite-rich amphibolite at contact with coarse-grained pegmatitic intrusion that features randomly orientated books of biotite. Mica-poor amphibolite is present in the lower part of the photo and is foliated; i) Tray 24 (~304.6 m) of TUR13DD005. Fine- to medium-grained metadolerite (pale green in centre) crosscutting at high angle a foliated and coarser grained amphibolite. The metadolerite is partly brecciated by later quartz–epidote±calcite vein networks; j) Tray 80 (613.90 m) in TUR13DD003, site of sample GSWA 228665. Coarse-grained, undeformed meta-olivine gabbro

Open to tight folding of the gneissic fabric is evident in some sections of drillcore (e.g. sillimanite-bearing migmatitic gneiss, Fig. 3c, occupying bottom of TUR13DD004 at 597.45 – 669.80 m; Fig. 2), presumably reflecting folding at larger, regional scales. However, the orientations of foliation and fold structures could not be determined because the drillcores are not orientated.

Granitic material hosted by metasedimentary rocks and those of unknown protolith commonly exist as boudinaged leucocratic layers and domains (Figs 3c–e, 4a–c, 6a–d,f). Contacts between these layers and domains and the melanosomes or layering in the host rocks vary from sharp and relatively planar to diffuse and highly irregular (Figs 3g,h, 4a,b,d, 6). These rocks are migmatites in which some leucosomes were injected and others may have formed by in situ melting. Leucosomes are interpreted as having formed in situ if they are evenly and regularly distributed throughout an interval (e.g. Fig. 3d), and commonly have diffuse margins against the melanosome host rock. If leucosomes are sparse and unevenly distributed within a given interval, they are interpreted to be injected melt (Fig. 4b,c). Regardless of the specific concentration of leucosomes in a particular interval of host rock, leucosomes are distributed throughout the non-mafic rock portion of drillcores and are typically up to 5 cm thick. Granitic rocks contain biotite and coarse-grained muscovite, attesting to temperatures for their production not exceeding the upper limit of muscovite stability. Granitic rocks, including pegmatites, are mildly to strongly peraluminous (ASI values of 1.04 – 2.48; median 1.35).

Leucosomes are commonly wrapped by or concordant with the micaceous fabric of the host rock, and where strain is lower and leucocratic material is abundant, the foliation is strongly anastomosing (e.g. Figs 3d, 6a,f). Granitic rocks (and pegmatites, see below) are sufficiently coarse-grained and leucocratic that they typically appear undeformed at the scale of the drillcore (Figs 3g, 4a,e). However, in thin section (not shown), quartz shows well-developed internal deformation and recrystallization features. Evidence for partial melting shows that metamorphic grade is at least upper amphibolite facies (Kelsey et al., 2022), and the injected melt suggests that the rocks were close to or locally above the solidus.

Leucogranitic pegmatite veins are common throughout the drillcores. Where mica is present, it is commonly coarse-grained — typically as books — although the rocks are dominated by coarse-grained to very coarse-grained quartz and feldspar (Figs 3c,g,h, 4a). Some pegmatites are muscovite-rich and do not contain biotite. Tourmaline and rare garnet occur in pegmatite. Numerous pegmatites are clearly intrusive into the host rock (e.g. Fig. 3g,h). A portable X-ray fluorescence spectrometer (pXRF) was used to search pegmatites for potential geochronology samples but all had low Zr concentrations (≤40 ppm), implying low modal abundance of zircon. Although their age is unknown, intrusive relationships indicate the pegmatites were synchronous with or post-dated gneissic fabric development, metamorphism and massive sulfide mineralization (see below). Pegmatites are up to ~14 m thick although the majority are considerably thinner (Fig. 2). No pluton-scale granitic or leucogranitic intervals are present in the drillcore. Rather, the occurrence is either that of intimate interlayering of thin leucocratic veins and host rock ('lit-par-lit'), or thicker pegmatitic veins.

All amphibolites (Figs 3g,i, 4a–c,f–h) are quartz-bearing and are variably retrogressed, with plagioclase and amphibole varying from fresh to pervasively replaced by undeformed intergrowths of clinozoisite–epidote and actinolite (not shown). Some amphibolites contain titanite and, in rare cases, biotite and chlorite are retrograde minerals. Garnet is rare and is mostly present adjacent to intervals of finely compositionally layered rock featuring centimetre-scale layers of massive sulfide minerals (mostly pyrrhotite, some pyrite and minor chalcopyrite) and clinopyroxene- and apatite-rich mineralogy and garnet–quartz rocks (Figs 3a, 4d). All these rock types are collectively classified as metamorphosed hydrothermal rock in the geological logs (Fig. 2). These amphibolites are much darker compared with the typical garnet-absent amphibolites. Garnet-bearing amphibolites are geochemically similar to the garnet-absent amphibolites, and both have unmodified MORB geochemistry (Fig. 5b). However, garnet-bearing amphibolites have lower Mg# (28–33), Al_2O_3 and CaO and more elevated ASI, TiO_2, P_2O_5, La, Y, Yb, Nb and Th concentrations than other amphibolites (Mg# 33–60). These sulfide-rich regions are concordant with compositional and deformational layering. A more complete account of metasomatism and alteration will be provided in a separate contribution.

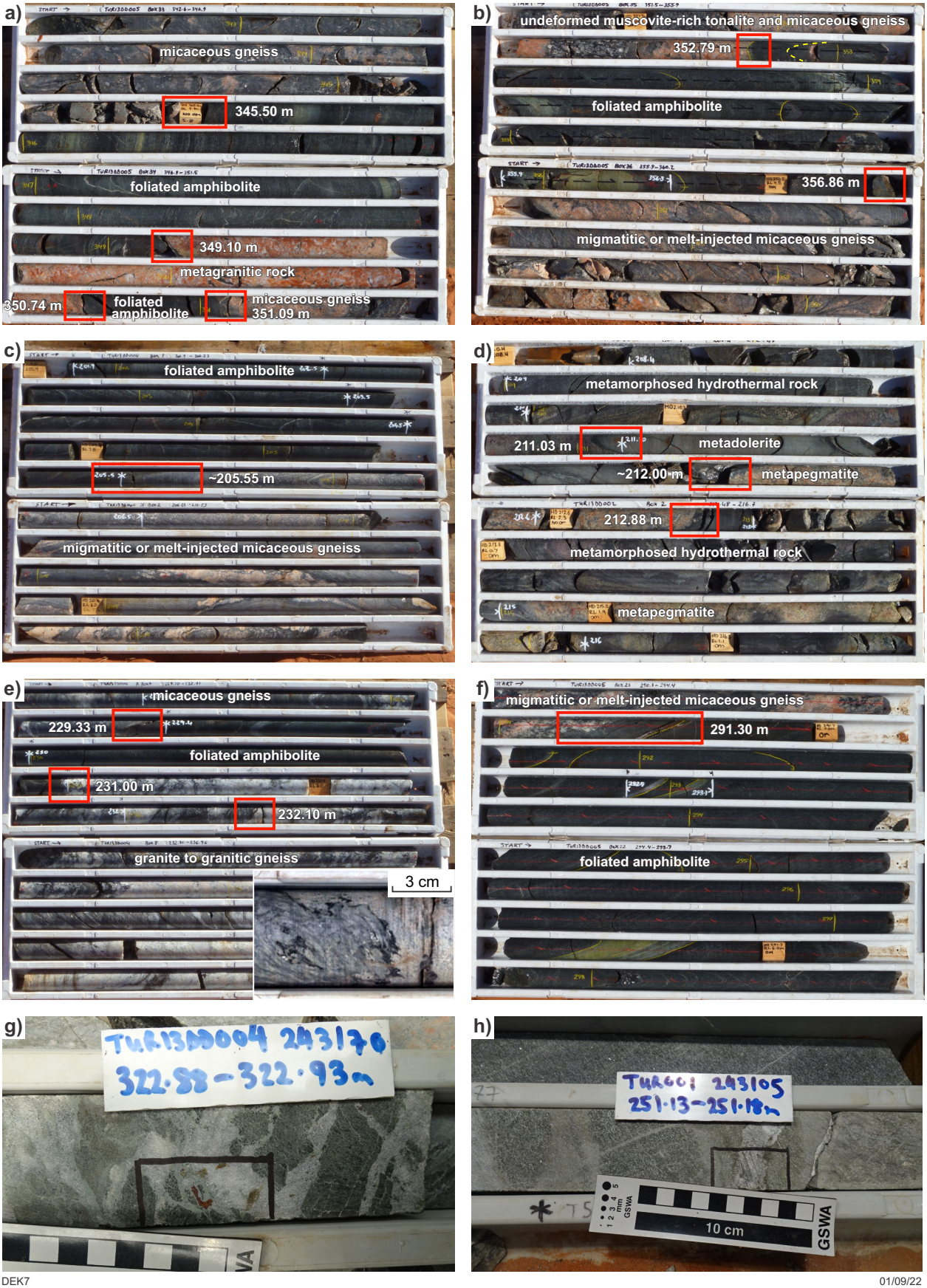
a)
micaceous gneiss
345.50 m
foliated amphibolite
349.10 m
metagranitic rock
350.74 m
foliated amphibolite
micaceous gneiss
351.09 m
b)
undeformed muscovite-rich tonalite and micaceous gneiss
352.79 m
foliated amphibolite
356.86 m
migmatitic or melt-injected micaceous gneiss
c)
foliated amphibolite
~205.55 m
migmatitic or melt-injected micaceous gneiss
d)
metamorphosed hydrothermal rock
211.03 m
metadolerite
~212.00 m
metapegmatite
212.88 m
metamorphosed hydrothermal rock
metapegmatite
e)
micaceous gneiss
229.33 m
foliated amphibolite
231.00 m
232.10 m
granite to granitic gneiss
3 cm
f)
migmatitic or melt-injected micaceous gneiss
291.30 m
foliated amphibolite
g)
TUR13DD004 243170
322.88 – 322.93m
h)
TUR001 243105
251.13 – 251.18m
10 cm
GSWA

DEK7 01/09/22

Figure 4. (page 7) Contact relationships between rock types in drillcore from Top Up Rise prospect. All photos except g and h are courtesy of Border Exploration Pty Ltd. In all photos except g and h the relationships described refer to locations marked by red boxes. Core diameter is 47.6 mm and trays are 1 m long. a) Trays 33 and 34 of TUR13DD005. Contact between weakly to moderately well-foliated, coarse-grained, muscovite-rich micaceous gneiss with well-foliated amphibolite, at 345.50 m. In the lower part of the photo, orange-coloured pegmatite is in sharp contact with foliated amphibolite, at 349.10 m and at 350.74 m. At 351.09 m, there is weakly to moderately deformed muscovite-rich micaceous gneiss and granite, likely intruding into the amphibolite; b) Trays 35 and 36 of TUR13DD005. Weakly deformed, coarse-grained, muscovite-rich gneiss and pegmatite intruded into foliated amphibolite, at 352.79 m. Broken contact between foliated amphibolite and foliated migmatitic or melt-injected micaceous gneiss, at 356.86 m. Yellow dashed line marks the trend of foliation; c) Trays 1 and 2 of TUR13DD004. Diffuse, foliation-parallel contact between amphibolite and migmatitic or melt-injected micaceous gneiss at ~205.55 m, which does not permit determination of a relative age relationship; d) Trays 1 and 2 of TUR13DD002. Metamorphosed hydrothermal rock featuring foliated layers of massive sulfide and garnet–quartz rock, crosscut by undeformed, younger metadolerite, at 211.03 m. The lower contact of the metadolerite with metapegmatite at ~212.00 m is obscured. Metadolerite with a sharp upper boundary with metapegmatite is at 212.88 m; e) Tray 7 (top) of TUR13DD004. Foliation-parallel contact between micaceous gneiss and mafic amphibolite, at 229.33 m, which does not permit determination of a relative age relationship. At 231.00 m and 232.10 m, there are contacts between metagranite intruding amphibolite. The inset shows a close-up of the contact at 232.10 m; f) Trays 21 and 22 of TUR13DD005. Foliation-parallel contact between foliated migmatitic or melt-injected micaceous gneiss and foliated amphibolite, at 291.30 m. Foliation-parallel zones of intense hydrothermal alteration marked by strong green epidote in 9th row are common in the amphibolite (e.g. ~297.40 m). Amphibolite is also dissected at high angle to foliation by numerous millimetre-scale veins of quartz–epidote±calcite; g) Tray 28 of TUR13DD004. Brecciation of amphibolite by quartz–chlorite-rich veins that may contain coarse-grained sulfide (chalcopyrite, inside black box). Site of sample GSWA 243170 (322.88 – 322.93 m); h) Tray 24 of TUR13DD001. Calcite-rich veins (wider one inside black box marked for thin section sample; the other narrower and to the right) and diffuse, local patches of more advanced alteration (to pale green epidote and actinolite) of amphibolite. Site of sample GSWA 243105 (251.13 – 251.18 m). For all vein types shown in this photo, sulfide mineralization is restricted to rare and finely disseminated grains

Coarse-grained, massive metagabbro is only in TUR13DD003 and is locally olivine-bearing (Figs 2, 3j). The rock is mostly fresh and retains an ophitic to intergranular texture of plagioclase and clinopyroxene. Alteration is typically minor, consisting of blue–green amphibole and epidote–clinozoisite replacing plagioclase and, less commonly, clinopyroxene. Olivine is mostly unaltered, although where partly or fully retrogressed, is replaced by a very fine-grained intergrowth of chlorite–tremolite–opaque Fe–Ti oxide±talc. Fractures within fresh olivine and along its margins contain abundant opaque Fe–Ti oxide minerals. Metagabbro and meta-olivine gabbro have weakly to moderately modified MORB geochemistry (Fig. 5b).

Metadolerites, typically tens of centimetres thick, are common in the drillcores, and are not foliated although are altered or retrogressed (Figs 2, 3i, 4d). In many cases they are clearly intrusive and crosscut the foliation in the host rocks (Figs 3i, 4d). These metadolerites are strongly altered or retrogressed from olivine–clinopyroxene–plagioclase to fine- to very fine-grained epidote–clinozoisite–actinolite. In rare cases, metadolerites contain a mylonitic fabric, for example where metadolerite occupies the contact between olivine metagabbro and psammitic gneiss at ~740 m in TUR13DD003 (Fig. 2). Metadolerites have an enriched, crustally contaminated signature (Fig. 5c) typical of other Australian intracontinental dolerites (e.g. Zhao et al., 1994; Wyborn et al., 1998; Li et al., 2006; Howard et al., 2007, 2015). The metadolerites crosscut and are therefore younger than metagabbro dated at c. 968 Ma (see below).

Veins that host minor sulfide mineralization are typically in amphibolites (more rarely in metagabbro and metadolerite) and are of three types (e.g. Fig. 4g,h). Although their relative timing is unclear, the three types are listed here in possible relative order from oldest to youngest:

1. quartz–chlorite veins associated with brecciation of amphibolite are fringed by minor K-feldspar and commonly contain coarse-grained chalcopyrite up to 5 mm in size. Visually, there is no obvious alteration halo around these veins

2. epidote–quartz-rich veins typically either exhibit well-developed alteration halos or are within areas of advanced, locally pervasive alteration involving epidote and actinolite (and locally chlorite). Some fine-grained, disseminated sulfide mineralization occurs within these veins

3. discrete calcite-rich veins are fringed by thin rinds of K-feldspar, and host rock alteration is restricted to extensive. These veins crosscut epidote–quartz-rich veins (type 2 above).

Contact relationships

Contact relationships are commonly obscured by deformation, alteration or broken and disintegrated drillcore. However, the following observations can be made:

1. The (modified) contacts between gneisses with unknown protoliths, amphibolites and metasedimentary rocks are parallel to the gneissic foliation (Fig. 4e,f), and none are observed to truncate that fabric.

2. Some metagranitic rocks — most notably leucogranite and pegmatite — exhibit intrusive contacts (e.g. Figs 3h, 4e) and clearly crosscut strong gneissic foliation in surrounding rocks (e.g. Figs 3g, 4a,b). Intrusive relationships show that at least some metagranite, mostly pegmatitic or leucogranitic rocks, are injected into host rock and feature apophyses or irregular margins (Figs 3c,h, 4e). However, many igneous contact relationships are unclear, either due to subsequent deformation or because the boundary is diffuse, as might be expected in the case of in situ melt generation (e.g. Figs 3c,d, 4a,c). The contact relationships for samples of granitic rock used for geochronology are shown in Figure 6.

3. Layers of massive sulfide mineralization and associated hydrothermal rocks are concordant with the gneissic fabric (Figs 3a, 4d).

4. Contacts between metagabbroic rocks and surrounding rocks are either strongly deformed or altered to mafic schist (e.g. Fig. 3f) or intruded by metadolerite (e.g. 735.40 – 742.60 m in TUR13DD003; Fig. 2).

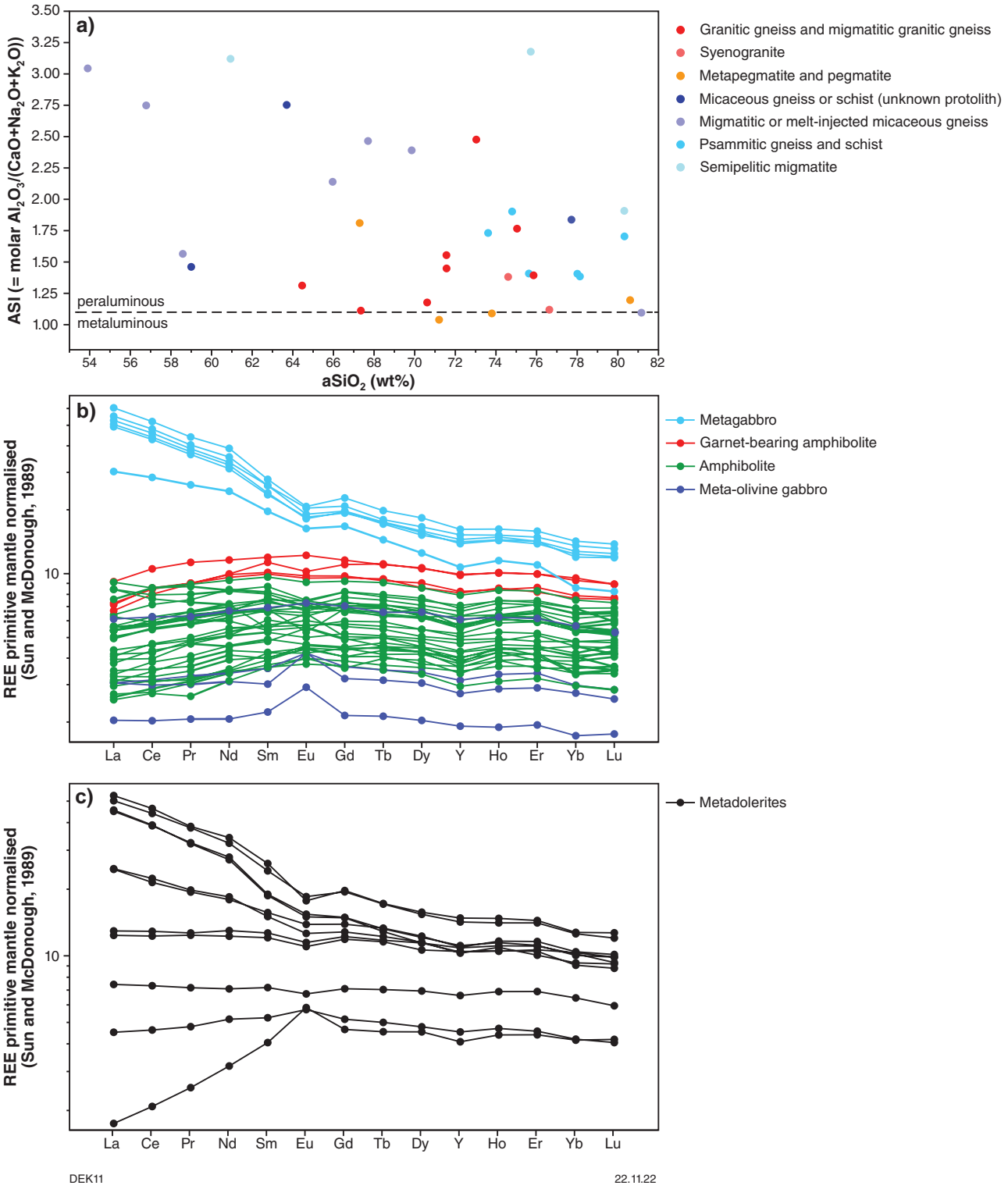

Figure 5. Geochemical summary plots for rocks from drillcore from the Top Up Rise prospect: a) anhydrous silica ($aSiO_2$) vs aluminium saturation index (ASI) for rocks with unknown protolith and metasedimentary rocks and all types of granitic rock samples; b) primitive mantle-normalised rare earth element plot for amphibolites, garnet-bearing amphibolites, metagabbro and meta-olivine gabbro samples; c) primitive mantle-normalised rare earth element plot for metadolerite samples

5. Metadolerite cuts across all other rock types, mostly at high angles, and typically is not deformed (e.g. Fig. 3i), although it is retrogressed and altered.

6. Veins, fractures and associated brecciation, alteration and some sulfide mineralization are common within some amphibolite intervals, but rare in other rocks (Fig. 4g,h). Metadolerite contains relatively few veins, suggesting that veining mostly pre-dated dolerite intrusion and that there may have been multiple stages of veining.

Geochronology

SHRIMP U–Pb zircon geochronology was conducted on 17 samples from four Top Up Rise prospect drillcores, including eight metagranitic rocks (Fig. 6), eight metasedimentary rocks and one metagabbro (Table 2). GSWA Geochronology Records have been published for 14 samples, and are summarized and reinterpreted below together with new results for three additional samples. The locations of the geochronology samples are shown on the drillcore logs in Figure 2.

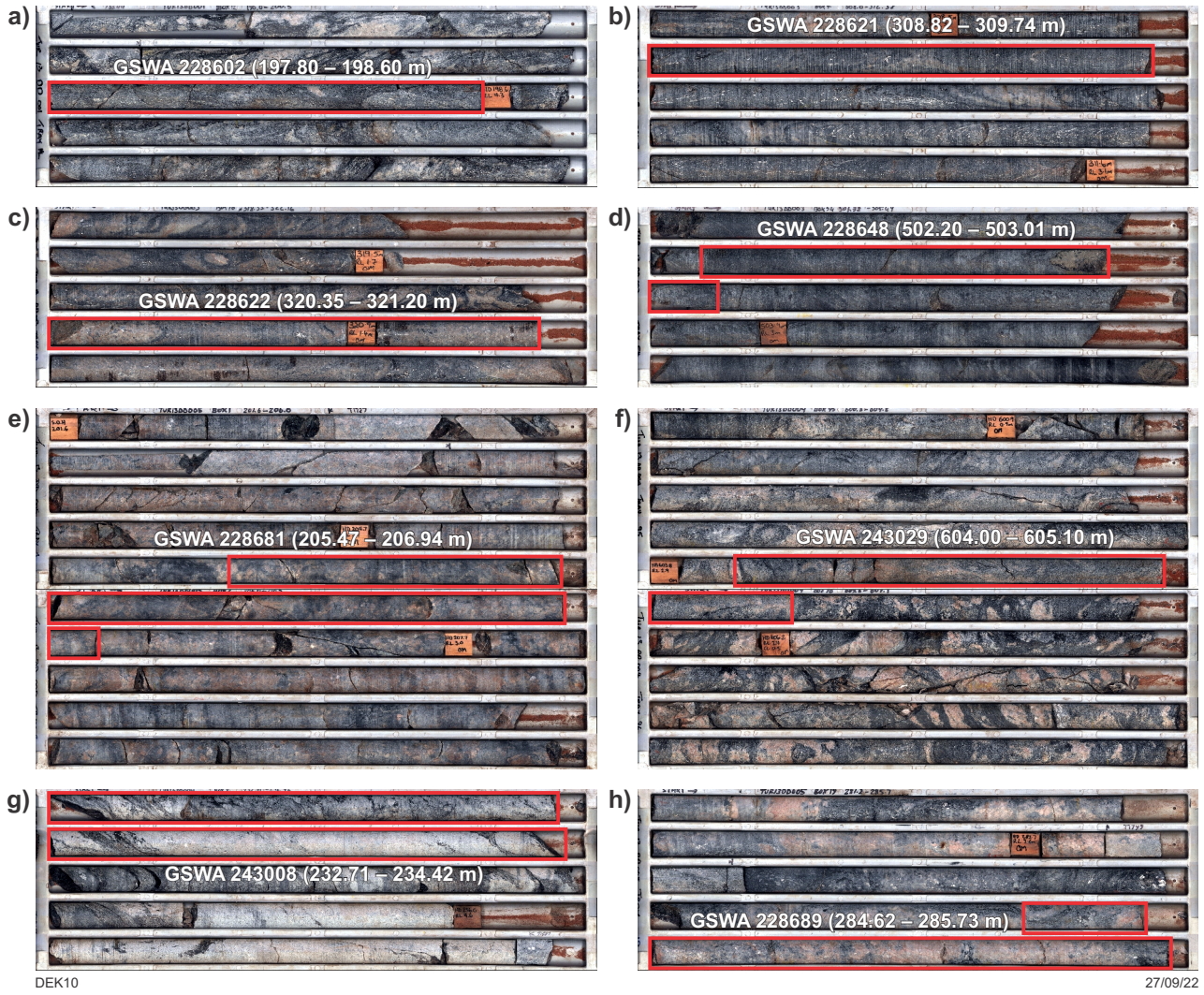

Figure 6. Contact relationships of dated granite samples. Location of six of eight granitic rocks that were dated by SHRIMP U–Pb zircon geochronology. All samples taken were of ½ or ¼ core and were located in the intervals marked by red boxes. All photos were taken with the HyLogger spectral scanner: a) Tray 12 of TUR13DD001, site of sample GSWA 228602. Migmatitic or melt-injected gneiss interlayered with leucocratic material. No intrusive contact. Strongly deformed; b) Tray 7 of TUR13DD003, site of sample GSWA 228621. No intrusive contact preserved; c) Tray 10 of TUR13DD003, site of sample GSWA 228622. More distinctly coarse-grained granitic interval, although no intrusive contact preserved; d) Tray 54 of TUR13DD003, site of sample GSWA 228648. Migmatitic gneiss or melt-injected gneiss interlayered with leucocratic material. No intrusive contact; e) Trays 1–2 of TUR13DD005, site of sample GSWA 228681. Coarse-grained granite containing a small proportion of mica-rich pockets. Upper contact is not present in the drillcore. Lower contact is at the end of Tray 3 (Tray 4 begins with amphibolite) and as such the nature of the contact is obscure. However, the amphibolite is far more strongly deformed than the granite, suggesting the granite is relatively late and intrusive; f) Trays 95–96 of TUR13DD004, site of sample GSWA 243029. Diffuse contact with host metasedimentary migmatite; g) Tray 8 of TUR13DD004, site of sample GSWA 243008. Strongly deformed and diffuse (upper) and sharp (lower) contact with mica-rich host; h) Tray 19 of TUR13DD005, site of sample GSWA 228689. Muscovite-rich granite that has diffuse contacts with host rock

Zircons in all samples, except the metagabbro sample GSWA 228652, consist of cores overgrown by high-uranium, low-thorium zircon rims (Fig. 7). Zircon cores in eight metagranitic samples (Table 2) yield very similar dates of c. 1880 to 1870 Ma, with an average of c. 1873 Ma (Fig. 8a), and relatively few older dates of 3044–1900 Ma. Many zircon cores in metagranitic samples exhibit truncated concentric zoning or broken edges, consistent with inheritance, possibly from a sedimentary protolith (e.g. Fig. 7). Detrital zircon cores in seven of eight samples of metasedimentary gneiss yield dates of 3074–1835 Ma, with a dominant age component at c. 1870 Ma, and maximum depositional ages (MDA) of c. 1877 to 1852 Ma (Fig. 8a, Table 2). One paragneiss sample (GSWA 228620) that yielded very few zircons (*n* = 15), indicates a conservative MDA of c. 2490 Ma, and a youngest single zircon core at 1838 Ma.

Uranium contents of zircon rims in 16 samples are mostly very high, with a median of 1322 ppm, and Th/U ratios are very low, with a median of 0.004 (Fig. 8b). Weighted mean sample ages for zircon rims range from 1624 to 1604 Ma, with one outlier at c. 1584 Ma based on preliminary data (Fig. 8a, Table 2). The mean ages are dispersed beyond analytical precision, suggesting that crystallization of zircon rims was protracted, or that some have lost radiogenic Pb, possibly as a consequence of radiation damage related to their high uranium content.

The youngest MDA for metasedimentary samples at the Top Up Rise prospect is 1852 ± 4 Ma, based on the 24 youngest zircon cores in GSWA 228680 (Fig. 8a, Table 2). Minor age components in metasedimentary samples include c. 2690, 2520–2450, 2050–2030, and 1980–1930 Ma. Together with the youngest age components at 1880– 1850 Ma, these detrital components are very similar to the 'Detrital P' signature recognized by Maidment et al. (2020, 2022) in widespread 1865–1835 Ma metasedimentary rocks throughout the NAC.

Understanding the zircon geochronology is not straightforward, and two main interpretations are possible. The preferred scenario is that the 1880–1870 Ma zircon cores in eight metagranitic samples are inherited, probably mainly from metasedimentary rocks, and 1624–1604 Ma zircon rims date incipient partial melting during metamorphism to generate the low-volume granitic rocks. Visual distinction between potential older granitic protoliths and younger leucosomes in drillcore is difficult, although possible granitic protoliths are at most a few metres thick within leucosome-rich rock (in situ and injected melt, or both), suggesting that the dated granitic gneiss is mostly leucosome. The centimetre-scale interlayering of granitic rock with metasedimentary host rock (Fig. 6) is more consistent with local partial melting and injection of leucosomes, or both, rather than more voluminous (i.e.

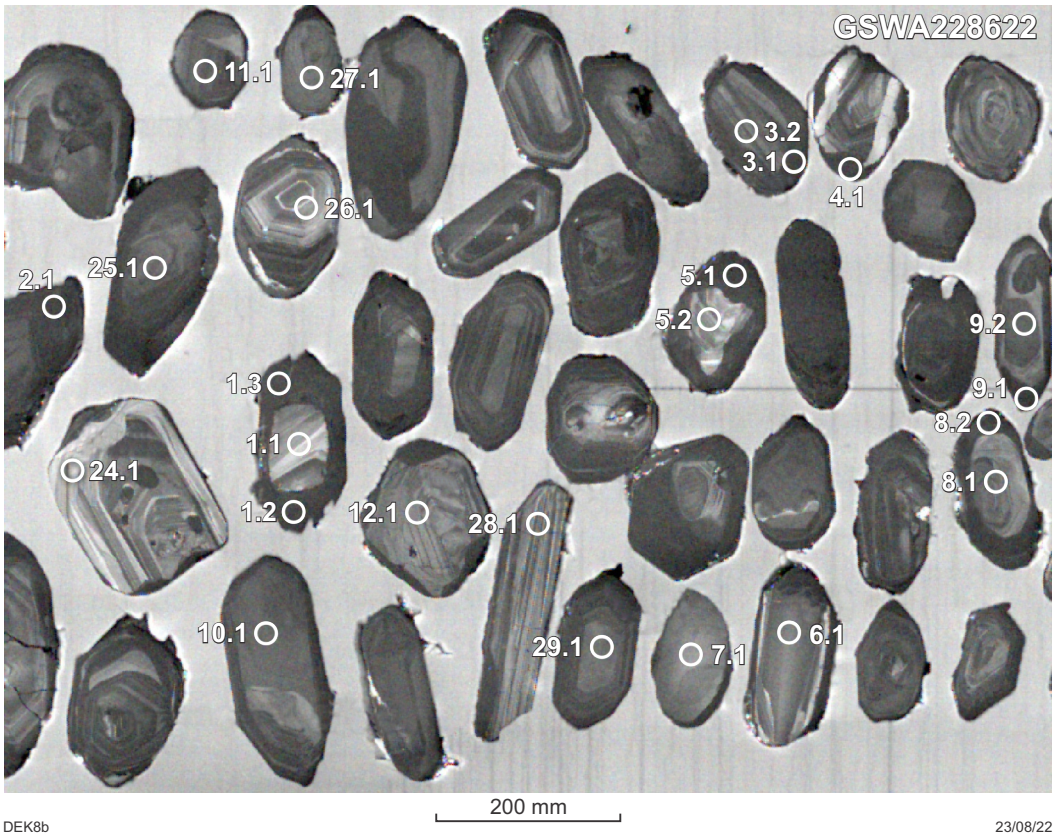

Figure 7. Cathodoluminescence (CL) image of representative zircon in granitic gneiss sample GSWA 228622 (Wingate et al., 2021e). For this sample zircon cores have youngest group weighted mean $^{207}Pb^*/^{206}Pb^*$ date 1880 ± 5 Ma and older group $^{207}Pb^*/^{206}Pb^*$ dates 3344–2013 Ma), and zircon rims have weighted mean $^{207}Pb^*/^{206}Pb^*$ date 1611 ± 5 Ma. Some zircon cores exhibit truncation of concentric zoning, and some others are broken, features consistent with an inherited origin for zircon cores in this sample. Numbered circles indicate the approximate locations of SHRIMP analysis sites

plutonic)intrusion. There is also no indication in the drillcores of (meta)sedimentary cover overlying granitic basement, although such a relationship could exist below or away from the drillcores.

Moreover, the metagranitic rocks are typically peraluminous to strongly peraluminous, S-type granites, and crystallization at 1880–1870 Ma would require them to have been derived by partial melting of pre-1880 Ma peraluminous source rocks. If so, the production of such large amounts of 1880– 1870 Ma zircon via partial melting of peraluminous source rock is unlikely, unless melting temperatures were well in excess of the solidus and melt volumes were significant (e.g. Piechocka et al., 2017, and references therein). However, coarse-grained muscovite in metasedimentary and granitic rocks indicates that temperatures associated with metamorphism and partial melting did not exceed the upper limit of muscovite stability (~700–750 °C; Kelsey et al., 2022), suggesting that melt volumes were low. Preservation of rare intrusive contacts between granitic and metasedimentary host rocks, as described above, implies that at least some magmatism clearly post-dated sedimentation.

Inherited zircons may be expected to dominate in peraluminous, S-type granites (e.g. Gulson and Krogh, 1973; Jeon et al., 2014). In such rocks at ~700–750 °C, zircon solubility is low (Harrison et al., 1999; Piechocka et al., 2017), hence the fraction of new zircon able to crystallize from melt would likely be low in comparison to the fraction of inherited zircon in melt. Indeed, the low solubility and thus low amount of magmatic zircon, which commonly manifests as rims on xenocrystic cores in peraluminous, leucocratic granitic rocks, has elsewhere complicated the dating of such rocks (e.g. Williams, 1992; Bea et al., 2007; Piechocka et al., 2017).

The alternative interpretation is that the zircon cores represent crystallization of a significant magmatic protolith at 1880–1870 Ma, that deposition of sediments was younger (consistent with a MDA of c. 1852 Ma), and that 1624–1604 Ma zircon rims date metamorphism and partial melting to produce relatively minor granitic leucosomes. However, the intimate interlayering style of granitic rock with metasedimentary host rock (Fig. 6) within the drillcores, rather than pluton-scale granitic rock or ubiquitous metasedimentary rocks overlying granite, is not strongly suggestive that a granitic basement–metasedimentary cover relationship was intersected (although its existence below or away from the drillcores remains plausible). It is worth noting that zircon rims in metasedimentary samples that do not contain leucosomes (e.g. psammitic gneiss samples GSWA 228680 and 228687) are identical in age, appearance, and U and Th composition to zircon rims in metagranitic samples (Fig. 8b). This suggests that all zircon rims formed under similar conditions during metamorphism and partial melting, consistent with the inferred low volumes of magma.

Our preferred interpretation is that the 1880–1870 Ma zircon cores in eight metagranitic samples are inherited and that partial melting to produce granitic leucosomes occurred at 1624–1604 Ma. In this interpretation, the source of 1880–1870 Ma zircons at Top Up Rise prospect and across the NAC remains unknown (Phillips et al., 2016; Maidment et al., 2020, 2022). In addition, because the dominant 1880–1865 Ma zircon component that defines the 'Detrital P' signature is throughout the NAC, it is not necessary that Top Up Rise prospect is near the source of those zircons. The similarity of zircon core ages in all Top Up Rise prospect samples to the 'Detrital P' age spectrum implies that the NAC extends westwards beneath the easternmost Canning Basin, at least as far as the Lasseter Shear Zone (see also Lu et al., 2022).

The youngest rock dated at the Top Up Rise prospect is a coarse-grained metagabbro that yielded a preliminary igneous crystallization age of c. 968 Ma (GSWA 228652, unpublished data). Apatite from this sample and from another lower interval in the same drillcore yields similar preliminary laser ablation inductively coupled plasma mass spectrometric (LA-ICP-MS) U–Pb intercept ages of c. 970 Ma (GSWA, unpublished data). This age is similar to the well-dated c. 975 Ma Central Desert Dolerite (sample GA 96496009, Wyborn, 1998), and possibly the poorly dated c. 1000 Ma Kullal Dolerite of the Musgrave Province (Glikson et al., 1996).

Geological history

Several observations and the geochronological data described above suggest the following evolution of crystalline basement rocks at Top Up Rise prospect:

1. Sedimentation was younger than c. 1852 Ma (MDA for GSWA 228680, Table 1), and a minimum age for deposition is provided by the 1624–1604 Ma age of metamorphism. The Top Up Rise prospect basin could correlate with the NAC-wide basin system into which 1865–1835 Ma turbiditic sediments were deposited (Crispe et al., 2007; Lambeck et al., 2012; Maidment et al., 2020, 2022). Alternatively, numerous periods of sedimentation into unnamed basins in the interval 1810–1630 Ma are known from the NAC (Scrimgeour, 2013a, b; Phillips et al., 2016), and protoliths to metasediments at Top Up Rise prospect could reflect deposition into one of these basins. Amphibolites may reflect mafic magmatism (?volcanism) coeval with sedimentation into the Top Up Rise prospect basin. The metasedimentary rocks contain abundant 1880–1870 Ma detritus and are similar to the 'Detrital P' age spectrum for the NAC. Based on the preferred interpretation that 1880–1870 Ma zircon cores do not represent igneous crystallization of significant granitic rocks at Top Up Rise prospect, sedimentation occurred prior to granitic magmatism, consistent with intrusive contacts that demonstrate that at least some magmatism post-dated sedimentation.

2. Compositional-layering- and foliation-parallel metasomatism and associated massive sulfide mineralization (e.g. various narrow intervals: 210.00 – 235.50 m in TUR13DD002; 326.63 – 328.90 m, 333.03 – 333.90 m, 338.12 – 339.50 m and 367.70 – 369.70 m in TUR13DD003; Figs 3a, 4d) post-dated sedimentation and pre-dated metamorphism, although this has not been dated precisely.

3. Deformation and metamorphism to upper amphibolite to lower granulite facies involved partial melting (e.g. GSWA 243004, Kelsey et al., 2022) and produced S-type granitic rocks at 1624–1604 Ma. Hydrothermal massive sulfide-bearing intervals were metamorphosed to gneisses and schists, including garnet-bearing amphibolites, which characterize these hydrothermal

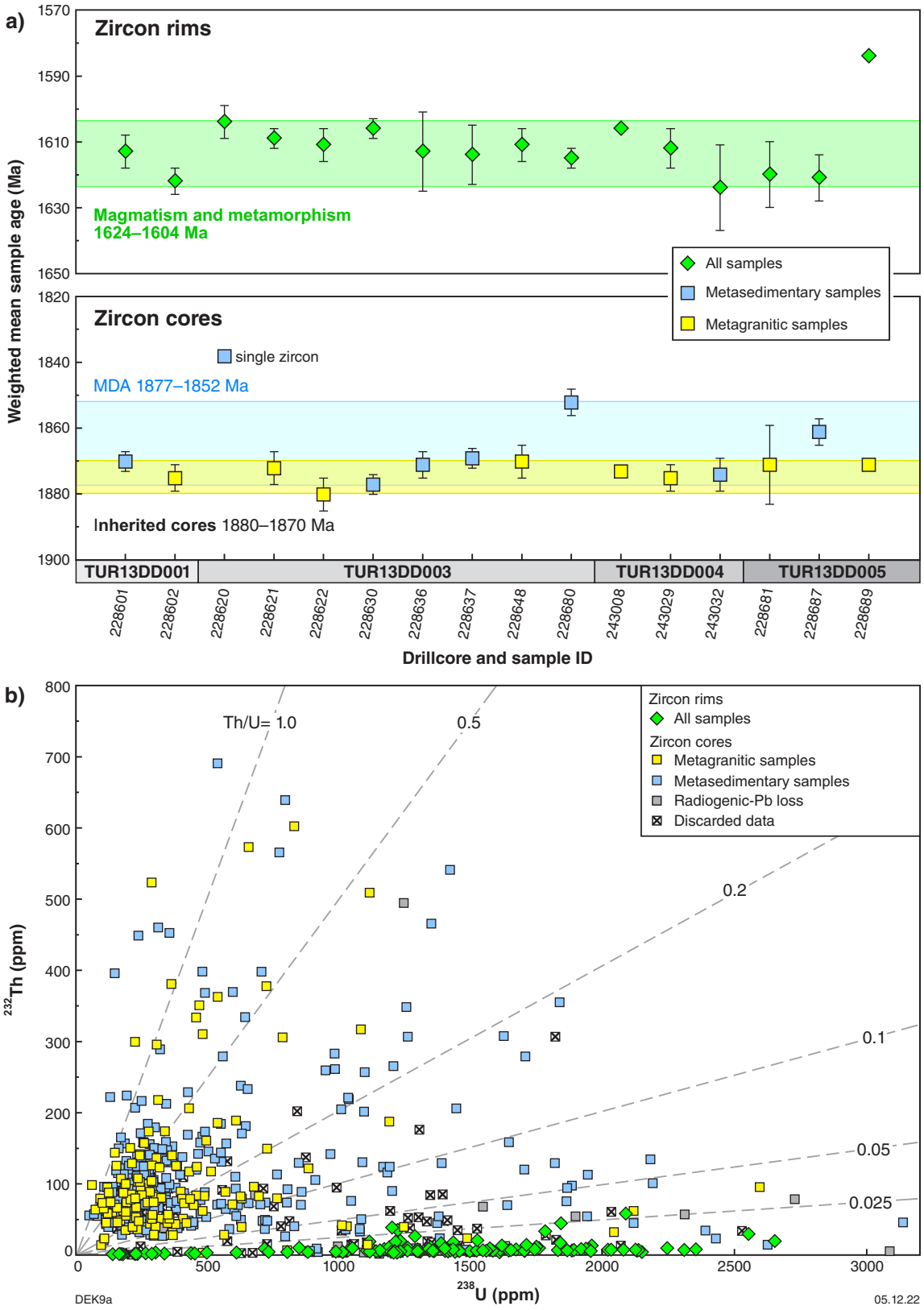

Figure 8. Top Up Rise prospect geochronology summaries: a) weighted mean ages of zircon rims during metamorphism and magmatism (upper panel), weighted mean sample ages for xenocrystic zircon cores in metagranitic rocks and maximum depositional ages (MDA) for metasedimentary rocks (both lower panel). Error bars indicate 95% confidence intervals. 'Single zircon' for sample GSWA 228620 is a single analysis as too few zircons were yielded to define a weighted mean group age for MDA in this sample. Green, blue and yellow shaded age intervals denote the range of weighted mean ages of the three age classifications across the sample set. Blue and yellow overlap in the lower panel; b) Thorium vs uranium ppm contents for all dated zircons show very low Th/U ratios (median 0.004) in rims in all samples

rocks. Folding of gneissic fabrics, leucosomes and granitic veins probably occurred at this time, which would mean that the generation of granitic leucosomes either pre-dated or was broadly synchronous with deformation at 1624–1604 Ma. Metamorphism at 1624–1604 Ma is slightly younger than the 1640–1630 Ma Liebig Orogeny and slightly older than the 1590–1570 Ma Chewings Orogeny (Scrimgeour, 2013a, b).

4. Intrusion of olivine gabbro and coarse-grained gabbro occurred at c. 968 Ma. Both have weakly modified MORB-like geochemistry comparable to that of the Central Desert and Kullal Dolerites. The relative timing of intrusion of olivine gabbro and coarse-grained gabbro to alteration is not clear. It is possible that the two are synchronous, although some or all alteration could post-date gabbroic magmatism as some veining does exist in gabbro.

5. Discordant quartz-, epidote- and calcite-rich veins were emplaced during alteration of host rocks to epidote, actinolite, chlorite, K-feldspar, quartz, hematite and some sulfide mineralization (Fig. 4g,h).

6. Metadolerites typically crosscut gneissic fabrics at high angles (Fig. 3i). The abundant veining typical of the amphibolites is not present in these rocks, hence the metadolerite probably post-dated brecciation and alteration. However, rare veins in metadolerite (e.g. Tray 38, TUR13DD003) suggest either a multi-stage alteration history or that (some?) dolerites were intruded prior to veining and brecciation and typically remained competent during this activity. Metadolerite intruded the meta-olivine gabbro and coarse-grained metagabbro, and therefore are younger than c. 968 Ma. There are geochemical similarities between these rocks and c. 825 Ma dolerites of the Willouran Large Igneous Province (e.g. Gairdner Dolerite, Zhao et al., 1994; Wingate et al., 1998), although the Top Up Rise prospect metadolerites are more enriched and crustally contaminated and contain a small negative Eu anomaly. An imperfect match for the geochemistry of metadolerite with the Gairdner Dolerite and Willouran Large Igneous Province does not allow unequivocal absolute age determination for the metadolerites by proxy. Metadolerite geochemistry is not similar to that of the c. 755 Ma Mundine Well Dolerite and equivalents, such as the Keene Basalt (Wingate and Giddings, 2000; Li et al., 2006; Zi et al., 2019).

7. Local to pervasive high-strain deformation (mylonitization; Fig. 3e,f) and widespread, pervasive retrogression produced epidote and actinolite in amphibolites and metadolerites and retrogressive feldspar and mica (largely sericite) in felsic rocks. Mylonite is present in metagabbros, metadolerite and other rocks, indicating that deformation was younger than dolerite intrusion. It is possible that mylonitization was related to the Petermann (630–520 Ma) or Alice Springs (450–295 Ma) Orogenies (Haines et al., 2001; Edgoose et al., 2004; Buick et al., 2008; Scrimgeour, 2013a; Kirkland et al., 2014a, b; Quentin de Gromard et al., 2016, 2017) or to initiation of the Canning Basin at c. 490 Ma (GSWA, 1990; Hocking, 1994; Normore et al., 2021; Wingate et al., 2021k), and likely reactivated older structures that existed within the Lasseter Shear Zone system.

Table 2. Summary of U–Pb geochronology of zircons from Top Up Rise prospect samples

Drillhole ID	*Sample ID*	*Lithology*	*Inheritance (Ma)*	*±*	*Maximum age of deposition (Ma)*	*±*	*Metamorphism and magmatism (Ma)*	*±*	*Reference*
TUR13DD001	228601	psammitic gneiss			1870	3	1613	5	Wingate et al., 2021a
	228602	granitic gneiss	1875	4			1622	4	Wingate et al., 2021b
TUR13DD003	228620	micaceous paragneiss			2490 (1838)	5	1604	5	Wingate et al., 2021c
	228621	granitic gneiss	1872	5			1609	3	Wingate et al., 2021d
	228622	granitic gneiss	1880	5			1611	5	Wingate et al., 2021e
	228630	garnet–biotite gneiss			1877	3	1606	3	Wingate et al., 2021f
	228636	garnet–biotite gneiss			1871	4	1613	12	Wingate et al., 2021g
	228637	migmatitic gneiss			1869	3	1614	9	Wingate et al., 2021h
	228648	granitic gneiss	1870	5			1611	5	Wingate et al., 2021i
	228680	psammitic gneiss			1852	4	1615	3	Wingate et al., 2021j
	228652	metagabbro	c. 968						GSWA, unpublished data
TUR13DD004	243008	metamonzogranite	c. 1873				c. 1606		GSWA, unpublished data
	243029	granitic gneiss	1875	4			1612	6	Wingate et al., 2022a
	243032	semipelitic migmatite			1874	5	1624	13	Wingate et al., 2022b
TUR13DD005	228681	metamonzogranite	1871	12			1620	10	Wingate et al., 2022c
	228687	psammitic gneiss			1861	4	1621	7	Wingate et al., 2022d
	228689	metasyenogranite	c. 1871				c. 1584		GSWA, unpublished data

NOTES: age uncertainties are 95% confidence intervals; inheritance refers to zircon cores

Conclusions

Crystalline rocks at the Top Up Rise prospect were intersected by exploration drilling and are currently the only available basement rock samples to study within the Lasseter Shear Zone system that underlies the eastern Canning Basin, west of the Aileron Province of the NAC. The rocks are varied in lithology and include upper amphibolite to lower granulite facies schists and gneisses (including in situ and melt-injected leucosomes), amphibolites and metagabbros. Alteration and sulfide mineralization attest to hydrothermal fluid flow during at least two stages of basement evolution. SHRIMP U–Pb zircon geochronology indicates mainly 1880–1870 Ma zircon cores in granitic rocks, and 3074–1825 Ma cores and maximum depositional ages of 1877–1852 Ma in metasedimentary rocks. Zircon rims in both granitic and metasedimentary rocks yield ages for metamorphism of 1624–1604 Ma, are highly enriched in uranium, and have very low Th/U ratios of about 0.004.

The age of granitic magmatism is recorded by zircon rims at 1624–1604 Ma, and the 1880–1870 Ma zircon cores in granitic rocks are interpreted to represent inheritance rather than crystallization of a granitic protolith. Zircons in the age range from 1880 to 1870 Ma are common as detrital components in 1865–1835 Ma metasedimentary rocks across the NAC, and Top Up Rise prospect zircon ages are very similar to the 'Detrital P' signature of Maidment et al. (2020). This indicates that the NAC continues westwards beneath the easternmost Canning Basin, at least as far as the Lasseter Shear Zone, although the intersected rocks at Top Up Rise prospect probably do not represent a source of 1880–1870 Ma zircons across the NAC. Massive metagabbro and meta-olivine gabbro were emplaced at c. 968 Ma, and metadolerites are even younger, although not dated. The geological evolution of the Top Up Rise prospect was protracted, and the latest event included high-strain deformation that overprinted earlier hydrothermal and alteration activity, including sulfide mineralization. It is possible that mylonitization could be Neoproterozoic or Paleozoic in age.

References

Bea, F, Montero, P, González-Lodeiro, F and Talavera, C 2007, Zircon inheritance reveals exceptionally fast crustal magma generation processes in Central Iberia during the Cambro-Ordovician: Journal of Petrology, v. 48, no. 12, p. 2327–2339, doi:10.1093/petrology/egm061.

Beyer, EE 2017, Nature and prospectivity of high-heat-producing granites of the central Aileron Province, Northern Territory: Northern Territory Geological Survey, Record 2017-004, 78p.

Beyer, EE, Hollis, JA, Whelan, JA, Glass, LM, Donnellan, N, Yaxley, G, Armstrong, R, Allen, C and Scherstén, A 2013, Summary of results, NTGS laser ablation ICPMS and SHRIMP U–Pb, Hf and O geochronology project: Pine Creek Orogen, Arunta Region, Georgina Basin and McArthur Basin, July 2008–May 2011: Northern Territory Geological Survey, Record 2012-007, 205p.

Braun, J, McQueen, H and Etheridge, M 1991, A fresh look at the Late Palaeozoic tectonic history of western-central Australia: Exploration Geophysics, v. 22, p. 49–54.

Buick, IS, Storkey, A and Williams, IS 2008, Timing relationships between pegmatite emplacement, metamorphism and deformation during the intra-plate Alice Springs Orogeny, central Australia: Journal of Metamorphic Geology, v. 26, no. 9, p. 915–936.

Close, DF, Scrimgeour, IR, Edgoose, CJ and Cross, A 2004, Late Palaeoproterozoic development of the SW margin of the North Australian Craton, *in* Dynamic Earth: past, present and future: Proceedings of the 17th Australian Geological Convention, Hobart, Tasmania: Geological Society of Australia, Abstracts, p. 149.

Crispe, AJ, Vandenberg, LC and Scrimgeour, IR 2007, Geological framework of the Archean and Paleoproterozoic Tanami Region, Northern Territory: Mineralium Deposita, v. 42, p. 3–26.

Doublier, MP, Johnson, SP, Gessner, KT, Howard, HM, Chopping, R, Smithies, RH, Martin, DMcB, Kelsey, DE, Haines, PW, Hickman, AH, Czarnota, K, Southby, C, Champion, DC, Huston, DL, Calvert, AJ, Kohanpour, F, Moro, P, Costelloe, R, Fomin, T and Kennett, BLN 2020, Basement architecture from the Pilbara Craton to the Aileron Province: new insights from deep seismic reflection line 18GA-KB1, *in* Exploring for the future: Extended abstracts *edited by* K Czarnota, IC Roach, S Abbott, M Haynes, N Kositcin, A Ray and E Slatter: Geoscience Australia, Canberra, p. 1–4.

Edgoose, CJ, Scrimgeour, IR and Close, DF 2004, Geology of the Musgrave Block, Northern Territory: Northern Territory Geological Survey, Report 15, 46p.

Frogtech Geoscience 2017, 2017 Canning Basin SEEBASE study and GIS data package: Geological Survey of Western Australia, Report 182, 297p.

Geological Survey of Western Australia (GSWA) 1990, Geology and mineral resources of Western Australia: Geological Survey of Western Australia, Memoir 3, 827p.

Glikson, AY, Stewart, AJ, Ballhaus, CG, Clarke, GL, Feeken, EHT, Leven, JH, Sheraton, JW and Sun, SS 1996, Geology of the western Musgrave Block, central Australia, with particular reference to the mafic-ultramafic Giles Complex: Australian Geological Survey Organisation, Bulletin 239, 206p.

Gulson, BL and Krogh, TE 1973, Old lead components in the young Bergell Massif, south-east Swiss Alps: Contributions to Mineralogy and Petrology, v. 40, p. 239–252.

Haines, PW, Hand, M and Sandiford, M 2001, Palaeozoic synorogenic sedimentation in central and northern Australia: a review of distribution and timing with implications for the evolution of intracontinental margins: Australian Journal of Earth Sciences, v. 48, p. 911–928.

Harrison, TM, Grove, M, McKeegan, KD, Coath, CD, Lovera, OM and Le Fort, P 1999, Origin and episodic emplacement of the Manaslu Intrusive Complex, Central Himalaya: Journal of Petrology, v. 40, no. 1, p. 3–19.

Hocking, RM 1994, Subdivisions of Western Australian Neoproterozoic and Phanerozoic sedimentary basins: Geological Survey of Western Australia, Record 1994/4, 85p.

Hollis, JA, Kirkland, CL, Spaggiari, CV, Tyler, IM, Haines, PW, Wingate, MTD, Belousova, EA and Murphy, RC 2013, Zircon U–Pb–Hf isotope evidence for links between the Warumpi and Aileron Provinces, west Arunta region: Geological Survey of Western Australia, Record 2013/9, 30p.

Howard, HM, Smithies, RH, Kirkland, CL, Kelsey, DE, Aitken, A, Wingate, MTD, Quentin de Gromard, R, Spaggiari, CV and Maier, WD 2015, The burning heart - the Proterozoic geology and geological evolution of the west Musgrave Region, central Australia: Gondwana Research, v. 27, no. 1, p. 64–94, doi:10.1016/j.gr.2014.09.001.

Howard, HM, Smithies, RH and Pirajno, F 2007, Geochemical and Nd isotopic signatures of mafic dykes in the western Musgrave Complex, *in* Geological Survey of Western Australia Annual Review 2005-06: Geological Survey of Western Australia, Perth, Western Australia, p. 64–71.

Jeon, H, Williams, IS and Bennett, VC 2014, Uncoupled O and Hf isotopic systems in zircon from the contrasting granite suites of the New England Orogen, eastern Australia: implications for studies of Phanerozoic magma genesis: Geochimica et Cosmochimica Acta, v. 146, p. 132–149.

Kelsey, DE, Korhonen, FJ, Romano, SS and Spaggiari, CV 2022, 243004: garnet-bearing pelitic schist, Top Up Rise prospect; Metamorphic History Record, <www.dmirs.wa.gov.au/MetamorphicHistory>.

Kirkland, CL, Wingate, MTD, Quentin de Gromard, R, Howard, HM and Smithies, RH 2014a, 205194: psammitic gneiss, Mitika Homestead; Geochronology Record 1203: Geological Survey of Western Australia, 5p., <www.dmirs.wa.gov.au/geochron>.

Kirkland, CL, Wingate, MTD, Quentin de Gromard, R, Howard, HM and Smithies, RH 2014b, 208414: quartzite, Mitika Homestead; Geochronology Record 1205: Geological Survey of Western Australia, 6p., <www.dmirs.wa.gov.au/geochron>.

Lambeck, A, Barovich, K, George, AD, Cross, A, Huston, D and Meixner, T 2012, Proterozoic turbiditic depositional system (Tanami Group) in the Tanami region, northern Australia, and implications for gold mineralization: Australian Journal of Earth Sciences, v. 59, p. 383–397.

Li, XH, Li, Z-X, Wingate, MTD, Chung, SL, Liu, Y, Lin, GC and Li, WX 2006, Geochemistry of the 755 Ma Mundine Well dyke swarm, northwestern Australia: part of a Neoproterozoic mantle superplume beneath Rodinia? Precambrian Research, v. 146, p. 1–15.

Lu, Y, Wingate, MTD, Smithies, RH, Gessner, K, Johnson, SP, Kemp, AIS, Kelsey, DE, Haines, PW, Martin, DM, Martin, L and Lindsay, M 2022, Preserved intercratonic lithosphere reveals Proterozoic assembly of Australia: Geology, v. 50, no. 10, p. 1202–1207, doi:10.1130/G50256.1.

Maidment, DW, Lu, Y, Phillips, C, Korhonen, FJ, Fielding, IOH, Wingate, MTD, Kirkland, CL, Murphy, R, Tilhac, R, Poujol, M and Zhao, J 2022, Geochronology of metasedimentary and igneous rocks in the Lamboo Province, Kimberley Region: reassessing collisional geodynamic models: Geological Survey of Western Australia, Report 215, 89p.

Maidment, DW, Wingate, MTD, Claoué-Long, JC, Bodorkos, S, Huston, D, Whelan, JA, Bagas, L, Lambeck, A and Lu, Y 2020, Geochronology of metasedimentary and granitic rocks in the Granites-Tanami Orogen: 1885–1790 Ma geodynamic evolution: Geological Survey of Western Australia, Report 196, 50p.

Marshall, D 2013, Final report for Exploration Incentive Scheme Funding DAG2012/00076897: E80/4427 Top Up project: Border Exploration Pty Ltd/ Corazon Mining Limited: Geological Survey of Western Australia, Statutory mineral exploration report A099481, <www.dmirs.wa.gov.au/wamex>, 31p.

Martin, DM, Murdie, RE, Kelsey, DE, Quentin de Gromard, R, Thomas, CM, Cutten, HN, Zhan, Y, Haines, PW and Brett, J 2022, Compilation and geological implications of the major crustal boundaries map and 3D model of Western Australia: Geological Survey of Western Australia, Record 2022/7, 49p.

Normore, L, Haines, PW, Carr, LK, Henson, P, Zhan, Y, Wingate, MTD, Zhen, YY, Lu, Y, Martin, S, Kelsey, D, Allen, H and Fielding, I 2021, Barnicarndy Graben, southern Canning Basin: stratigraphy defined by the Barnicarndy 1 stratigraphic well: The APPEA Journal, v. 61, no. 1, p. 224–235, doi:10.1071/AJ20160.

Phillips, C, Orth, K, Hollis, JA, Kirkland, CL, Bodorkos, S, Kemp, AIS, Wingate, MTD, Lu, Y, Iaccheri, L and Page, RW 2016, Geology of the Eastern Zone of the Lamboo Province, Halls Creek Orogen, Western Australia: Geological Survey of Western Australia, Report 164, 57p.

Piechocka, AM, Gregory, CJ, Zi, J-W, Sheppard, S, Wingate, MTD and Rasmussen, B 2017, Monazite trumps zircon: applying SHRIMP U–Pb geochronology to systematically evaluate emplacement ages of leucocratic, low-temperature granites in a complex Precambrian orogen: Contributions to Mineralogy and Petrology, v. 172, no. 8, p. 63, doi:10.1007/s00410-017-1386-5.

Quentin de Gromard, R, Howard, HM, Kirkland, CL, Smithies, RH, Wingate, MTD and Jourdan, F 2017, Post-Giles Event evolution of the Musgrave Province constrained by (multi-method) thermochronology, *in* GSWA 2017 extended abstracts: promoting the prospectivity of Western Australia: Geological Survey of Western Australia, Record 2017/2, p. 42–47.

Quentin de Gromard, R, Wingate, MTD, Kirkland, CL, Howard, HM and Smithies, RH 2016, Geology and U–Pb geochronology of the Warlawurru Supersuite and MacDougall Formation in the Mitika and Wanarn areas, west Musgrave Province: Geological Survey of Western Australia, Record 2016/4, 29p.

Scrimgeour, IR 2013a, Chapter 12: Aileron Province, *in* Geology and mineral resources of the Northern Territory *compiled by* M Ahmad and TJ Munson: Northern Territory Geological Survey, Special Publication, no. 5, 74p.

Scrimgeour, IR 2013b, Chapter 13: Warumpi Province, *in* Geology and mineral resources of the Northern Territory *compiled by* M Ahmad and TJ Munson: Northern Territory Geological Survey, Special Publication, no. 5, 21p.

Scrimgeour, IR, Close, DF and Edgoose, CJ 2005a, Mount Liebig, Northern Territory, SF 52-16: Explanatory notes: Northern Territory Geological Survey, 1:250 000 geological map series explanatory notes, 64p.

Scrimgeour, IR, Kinny, PD, Close, DF and Edgoose, CJ 2005b, High-T granulites and polymetamorphism in the southern Arunta Region, central Australia: Evidence for a 1.64 Ga accretional event: Precambrian Research, v. 142, no. 1–2, p. 1–27, doi:10.1016/j.precamres.2005.08.005.

Sun, S-S and McDonough, WF 1989, Chemical and isotopic systematics of oceanic basalts: implications for mantle composition and processes, *in* Magmatism in the Ocean Basins *edited by* AD Saunders and MJ Norry: The Geological Society of London, Special Publication 42, p. 313–345.

Williams, IS 1992, Some observations on the use of zircon U–Pb geochronology in the study of granitic rocks: Earth and Environmental Science Transactions of the Royal Society of Edinburgh, v. 83, no. 1-2, p. 447–458.

Wingate, MTD, Campbell, IH, Compston, W and Gibson, GM 1998, Ion microprobe U–Pb ages for Neoproterozoic basaltic magmatism in south-central Australia and implications for the breakup of Rodinia: Precambrian Research, v. 87, p. 135–159.

Wingate, MTD and Giddings, JW 2000, Age and paleomagnetism of the Mundine Well dyke swarm, Western Australia: implications for an Australia–Laurentia connection at 755 Ma: Precambrian Research, v. 100, p. 335–357.

Wingate, MTD, Lu, Y, Fielding, IOH, Kelsey, DE and Spaggiari, CV 2021a, 228601: paragneiss, Top Up Rise prospect; Geochronology Record 1714: Geological Survey of Western Australia, 7p., <www.dmirs.wa.gov.au/geochron>.

Wingate, MTD, Lu, Y, Fielding, IOH, Kelsey, DE and Spaggiari, CV 2021b, 228602: granitic gneiss, Top Up Rise prospect; Geochronology Record 1715: Geological Survey of Western Australia, 7p., <www.dmirs.wa.gov.au/geochron>.

Wingate, MTD, Lu, Y, Fielding, IOH, Kelsey, DE and Spaggiari, CV 2021c, 228620: paragneiss, Top Up Rise prospect; Geochronology Record 1716: Geological Survey of Western Australia, 6p., <www.dmirs.wa.gov.au/geochron>.

Wingate, MTD, Lu, Y, Fielding, IOH, Kelsey, DE and Spaggiari, CV 2021d, 228621: granitic gneiss, Top Up Rise prospect; Geochronology Record 1717: Geological Survey of Western Australia, 6p., <www.dmirs.wa.gov.au/geochron>.

Wingate, MTD, Lu, Y, Fielding, IOH, Kelsey, DE and Spaggiari, CV 2021e, 228622: granitic gneiss, Top Up Rise prospect; Geochronology Record 1718: Geological Survey of Western Australia, 6p., <www.dmirs.wa.gov.au/geochron>.

Wingate, MTD, Lu, Y, Fielding, IOH, Kelsey, DE and Spaggiari, CV 2021f, 228630: paragneiss, Top Up Rise prospect; Geochronology Record 1719: Geological Survey of Western Australia, 7p., <www.dmirs.wa.gov.au/geochron>.

Wingate, MTD, Lu, Y, Fielding, IOH, Kelsey, DE and Spaggiari, CV 2021g, 228636: paragneiss, Top Up Rise prospect; Geochronology Record 1720: Geological Survey of Western Australia, 7p., <www.dmirs.wa.gov.au/geochron>.

Wingate, MTD, Lu, Y, Fielding, IOH, Kelsey, DE and Spaggiari, CV 2021h, 228637: paragneiss, Top Up Rise prospect; Geochronology Record 1721: Geological Survey of Western Australia, 7p., <www.dmirs.wa.gov.au/geochron>.

Wingate, MTD, Lu, Y, Fielding, IOH, Kelsey, DE and Spaggiari, CV 2021i, 228648: granitic gneiss, Top Up Rise prospect; Geochronology Record 1722: Geological Survey of Western Australia, 6p., <www.dmirs.wa.gov.au/geochron>.

Wingate, MTD, Lu, Y, Fielding, IOH, Kelsey, DE and Spaggiari, CV 2021j, 228680: paragneiss, Top Up Rise prospect; Geochronology Record 1723: Geological Survey of Western Australia, 7p., <www.dmirs.wa.gov.au/geochron>.

Wingate, MTD, Lu, Y, Fielding, IOH, Kelsey, DE and Spaggiari, CV 2022a, 243029: granitic gneiss, Top Up Rise prospect; Geochronology Record 1845: Geological Survey of Western Australia, 5p., <www.dmirs.wa.gov.au/geochron>.

Wingate, MTD, Lu, Y, Fielding, IOH, Kelsey, DE and Spaggiari, CV 2022b, 243032: sillimanite–K-feldspar paragneiss, Top Up Rise prospect; Geochronology Record 1846: Geological Survey of Western Australia, 7p., <www.dmirs.wa.gov.au/geochron>.

Wingate, MTD, Lu, Y, Fielding, IOH, Kelsey, DE and Spaggiari, CV 2022c, 228681: metamonzogranite, Top Up Rise prospect; Geochronology Record 1843: Geological Survey of Western Australia, 5p., <www.dmirs.wa.gov.au/geochron>.

Wingate, MTD, Lu, Y, Fielding, IOH, Kelsey, DE and Spaggiari, CV 2022d, 228687: psammitic gneiss, Top Up Rise prospect; Geochronology Record 1844: Geological Survey of Western Australia, 8p., <www.dmirs.wa.gov.au/geochron>.

Wingate, MTD, Lu, Y, Fielding, IOH, Normore, LS and Haines, PW 2021k, 237996: quartz sandstone, Barnicarndy 1; Geochronology Record 1741: Geological Survey of Western Australia, 6p., <www.dmirs.wa.gov.au/geochron>.

Wong, BL, Morrissey, LJ, Hand, M, Fields, CE and Kelsey, DE 2015, Grenvillian-aged reworking of late Palaeoproterozoic crust of the southern North Australian Craton, central Australia: implications for the assembly of Mesoproterozoic Australia: Precambrian Research, v. 270, p. 100–123.

Wyborn, LAI, Hazell, M, Page, R, Idnurm, M and Sun, S-S 1998, A newly discovered major Proterozoic granite-alteration system in the Mount Webb region, central Australia, and implications for Cu–Au mineralisation: Australian Geological Survey Organisation, Research Newsletter 28, p. 1–6.

Zhan, Y 2018, A seismic interpretation of the southwestern Canning Basin, Western Australia: Geological Survey of Western Australia, Report 178, 34p.

Zhao, J-X, McCulloch, MT and Korsch, RJ 1994, Characterisation of a plume-related ~800 Ma magmatic event and its implications for basin formation in central-southern Australia: Earth and Planetary Science Letters, v. 121, no. 3-4, p. 349–367, doi:10.1016/0012-821X(94)90077-9.

Zi, J-W, Haines, PW, Wang, X-C, Jourdan, F, Rasmussen, B, Halverson, GP, Sheppard, S and Li, C-F 2019, Pyroxene $^{40}Ar/^{39}Ar$ dating of basalt and applications to large igneous provinces and Precambrian stratigraphic correlations: Journal of Geophysical Research: Solid Earth, v. 124, 18p., doi:10.1029/2019JB017713.

RECORD 2022/17

CRYSTALLINE BASEMENT BENEATH THE EASTERN CANNING BASIN AT THE TOP UP RISE PROSPECT

DE Kelsey, MTD Wingate, CV Spaggiari, RH Smithies, IOH Fielding, Y Lu, JK Porter and EG Finch

Access GSWA products

All products
All GSWA products are free to download as PDFs from the DMIRS eBookshop <www.dmirs.wa.gov.au/ebookshop>.
View other geoscience information on our website <www.dmirs.wa.gov.au/gswa>.

Hard copies
Limited products are available to purchase as hard copies from the First Floor Counter at Mineral House or via the DMIRS eBookshop <www.dmirs.wa.gov.au/ebookshop>.

Fieldnotes
Fieldnotes is a free digital-only quarterly newsletter which provides regular updates to the State's exploration industry and geoscientists about GSWA's latest programs, products and services.
Access by subscribing to the GSWA eNewsletter <www.dmirs.wa.gov.au/gswaenewsletter> or downloading the free PDF from the DMIRS eBookshop <www.dmirs.wa.gov.au/ebookshop>.

GSWA eNewsletter
The GSWA eNewsletter is an online newsletter that contains information on workshops, field trips, training and other events.
To keep informed, please subscribe <www.dmirs.wa.gov.au/gswaenewsletter>.

Further details of geoscience products are available from:

First Floor Counter
Department of Mines, Industry Regulation and Safety
100 Plain Street
EAST PERTH WESTERN AUSTRALIA 6004
Phone: +61 8 9222 3459 Email: publications@dmirs.wa.gov.au
www.dmirs.wa.gov.au/GSWApublications